PHYSICAL REVIEW B **83**, 201103(R) (2011)

Enhanced optical generation and detection of acoustic nanowaves in microcavities

N. D. Lanzillotti-Kimura,[1,*] A. Fainstein,[1] B. Perrin,[2] B. Jusserand,[2] L. Largeau,[3] O. Mauguin,[3] and A. Lemaitre[3]

[1]*Centro Atómico Bariloche & Instituto Balseiro, C.N.E.A., R8402AGP S. C. de Bariloche, Río Negro, Argentina*

[2]*Institut des NanoSciences de Paris, UMR 7588 CNRS - Université Paris VI, 75252 Paris cedex 05, France*

[3]*Laboratoire de Photonique et de Nanostructure, CNRS, Route de Nozay, 91460 Marcoussis, France*

(Received 5 March 2011; revised manuscript received 14 April 2011; published 25 May 2011)

The enhancement of the ultrafast coherent generation and detection of acoustic phonons in an optical microcavity is experimentally studied. We report pump-probe terahertz ultrasonic experiments in an optical microcavity as a function of laser energy and probe incidence angle. By tuning the laser wavelength to resonate with the microcavity mode at normal incidence and simultaneously varying the incidence angle of the probe beam we achieve a double optical enhancement. Under this condition both the coherent generation and detection of acoustic nanowaves are strongly enhanced. We demonstrate the use of optical microcavities as a promising tool to study acoustic phonons in reduced dimensions with increased sensitivity.

DOI: 10.1103/PhysRevB.83.201103 PACS number(s): 78.67.Pt, 63.22.Np, 78.20.hb, 78.20.hc

An optical microcavity confines the electromagnetic field both spectrally and spatially, inducing strong changes in the light–matter interaction and giving rise to novel physical phenomena and devices.[1–5] In the case of planar semiconductor optical microcavities, two distributed Bragg reflectors (DBRs) enclose an optical spacer.[5] Optical microcavities have been the subject of very active research during the last 15 years, and have been used to study the modification of the photonic lifetimes,[6] parametric oscillations,[3] cavity polariton Bose-Einstein condensates,[7,8] the polariton laser,[9,10] and amplification of Raman scattering signals,[11–13] among others. Here we experimentally study the signal enhancement in coherent phonon generation using optical microcavities.

The photonic confinement and amplification have been used in these high-Q resonators to amplify the optical generation of incoherent phonons through Raman processes and to prove effects in the phonon physics and dynamics in semiconductor nanostructures.[11–17] The optical resonances can be complemented with electronic resonances giving rise to amplified Raman cross sections of up to 10^7. On the contrary, the use of optical confinement for the enhanced coherent generation of acoustic phonons (in contrast with incoherent generation by spontaneous Raman scattering) is a concept that has been rarely treated up to now. The realization of a monochromatic, coherent, and intense source of ultrahigh frequency acoustic phonons[18–20] is only one of its potential applications. In coherent phonon generation experiments a femtosecond laser pulse (pump) generates coherent subterahertz phonons in a structure. These phonons modulate the optical properties of the sample. Finally, a second, delayed, and less intense laser pulse (probe) detects the time-dependent optical reflectivity.[21] The coherent generation of acoustic phonons using ultrafast lasers is characterized by a low efficiency in the light–hypersound transduction. In a previous work we demonstrated that planar optical microcavities can be used in coherent generation experiments;[22] we showed indications of signal enhancement as the optical resonance was approached and the modification of the selection rules in the phonon generation-detection process. Maris and co-workers[23] proposed a similar scheme using external microcavities to study systems with small photoelastic constants, presenting an alternative tool to the interferometric detection introduced by Perrin *et al.*[24] The modulation of optical microcavity modes, on the other hand, has been studied by the injection of hypersound pulses in both the polaritonic and the optic regimes.[25–27] Similarly, surface acoustic waves have been used to modulate optical microcavities and to control cavity polaritons.[28–30] In this work we present results of coherent phonon generation experiments in an acoustic nanocavity embedded in an optical microcavity under optical resonance conditions. It has been theoretically shown that the maximum amplification of the coherent generation and detection using microcavities cannot be reached simultaneously when the pump and probe beams have the same wavelength and angle of incidence.[31] In fact, when the laser is tuned with the cavity mode, although the coherent phonon generation efficiency reaches its maximum, the detection is an absolute zero.[32] Taking advantage of the light dispersion in microcavities, we introduce a strategy to achieve simultaneously the maximum amplification of both the generation and the detection of coherent acoustic phonons. We analyze the dependence of the microcavity efficiency on the laser wavelength and angle of incidence.

The studied sample consists of a planar semiconductor optical microcavity grown on a 001 oriented GaAs substrate by molecular beam epitaxy. A scheme of the sample can be found in Fig. 1(a). The optical microcavity is composed of two distributed Bragg reflectors (DBRs) enclosing a spacer. The top (bottom) DBR is composed of 3 (10) periods of $Ga_{0.8}Al_{0.2}As$/AlAs 55.39/64.19 nm, corresponding to a ($\lambda_l/4$, $\lambda_l/4$) multilayer. Here λ_l is the resonant wavelength of the microcavity. We choose a different number of periods in the DBRs to get a symmetric cavity mode by compensating the difference between the indices of refraction of air and the GaAs substrate. The Q factor of the optical microcavity is around 60, allowing 80-fs light pulses to enter in the resonator mode without being filtered. An acoustic nanocavity[14,17,20,33] acts as the $2\lambda_l$ spacer of the optical microcavity. The coherent generation and detection of the phonons of the latter structure will be the subject of the present study.

The acoustic nanocavity is formed by two phonon mirrors (PM); each reflector is formed by 13 bilayers of GaAs/AlAs 5.75/2.27 nm, corresponding to ($3\lambda_{ph}/4$, $\lambda_{ph}/4$) stacks.[34] A $3\lambda_{ph}/2$ GaAs layer constitutes the spacer between the two PMs. Here λ_{ph} is the acoustic resonant wavelength. The electronic

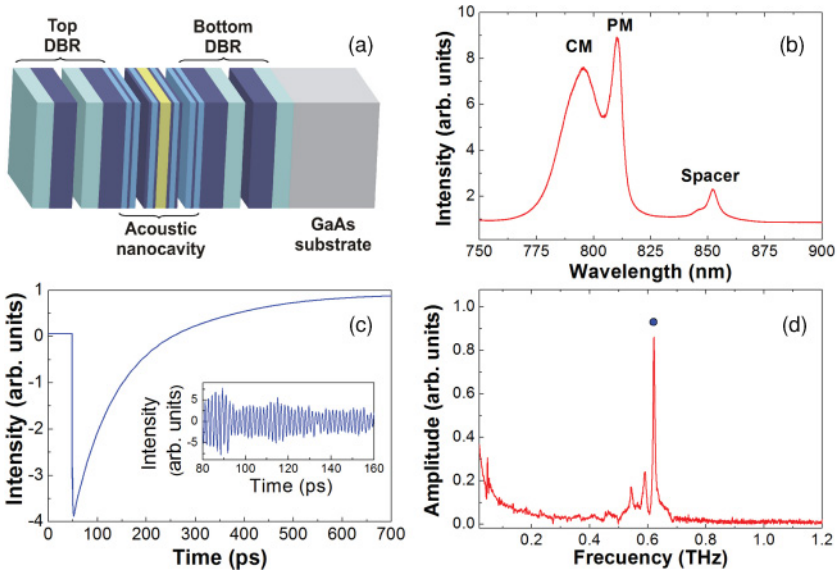

FIG. 1. (Color online) Optical microcavity. (a) Schematics of the structure. An acoustic nanocavity embedded in the optical microcavity. (b) Photoluminescence spectrum of the sample measured at room temperature using a He-Ne laser as excitation. CM, PM and Spacer stand for optical cavity mode and the luminescence peaks associated to the phonon mirrors acoustic spacer, respectively. (c) Time trace measured at room temperature using a laser wavelength $\lambda = 758$ nm. The time derivative of the signal between 80 and 160 ps is shown in the inset. (d) Fourier transform of the time trace shown in (c). The confined acoustic cavity mode is indicated with a solid circle.

transitions of the GaAs quantum wells forming the mirrors have higher energies than that of the acoustic spacer because of electronic confinement effects.

Figure 1(b) shows the photoluminescence spectrum of the microcavity measured at room temperature using an excitation wavelength $\lambda = 647.5$ nm. At this wavelength the optical DBRs are transparent although the quantum wells in the optical spacer absorb light. At 795 nm a broad peak can be observed (labeled as CM) corresponding to the light emission through the optical microcavity mode. At 810 and 853 nm the luminescence peaks associated with the exciton transitions at the phonon mirrors (PM) and acoustic spacer (Spacer) quantum wells can be identified. The sample was grown with a thickness gradient, and thus the CM can be displaced to shorter wavelengths by changing the spot on the surface of the sample. The reported pump-probe experiments were performed with this CM shifted to 758 nm to separate optical from excitonic resonance effects. Note that the CM is located at higher energies than the electronic transitions of the quantum wells forming the acoustic nanocavity.[36] This results in a reduced quality factor of the optical cavity as we will discuss later.

We performed standard pump-probe coherent phonon generation experiments on the optical microcavity.[21] We used a Ti-sapphire laser delivering 80 fs NIR light pulses, at a repetition rate of 80 MHz. The pump beam was modulated at 1 MHz in order to allow the synchronous detection with a lock-in amplifier. Pump and probe beams are cross polarized in order to allow a better filtering and improve the signal to noise ratio. Typical powers of 60 mW (20 mW) for the pump (probe) beam were used. We focused both beams onto an approximately 60 μm diameter spot. The collected time traces were 700 ps long. In Fig. 1(c) the time resolved reflectivity measured in the optical microcavity with the laser tuned with the optical mode is presented. At 50 ps the coincidence in time between the pump and probe pulses can be identified by a strong change in the reflectivity due to the electronic excitation of the sample. The coherent and monochromatic character of the phonon-induced variations in the reflectivity can be appreciated in the inset, where we present a detail of the derivative of the signal between 80 and 160 ps after the application of a bandpass filter. By Fourier transforming the time-dependent optical reflectivity, it is possible to recover the spectrum of acoustic excitations generated in the sample. Figure 1(d) shows the Fourier transform of the time derivative of the signal presented in Fig 1(c). An intense peak (indicated with a solid circle) can be identified at 620 GHz, along with side oscillations. This mode corresponds to confined acoustic phonons in the spacer of the acoustic nanocavity.[14] The spectrum shape is robust and remains unmodified when the laser is tuned around the CM.

The efficiency in the generation of coherent phonons using an optical microcavity is maximum when the excitation laser is tuned with the cavity mode, that is, when the electric field presents its maximum amplification.[23,31] The generated phonons within the optical microcavity modulate the index of refraction (or equivalently, the thickness) of the optical spacer, changing the cavity mode energy. The detection is directly related to a differential reflectivity measurement. Thus the detection sensitivity presents two maxima that coincide with the extremes of the derivative of the microcavity mode.[23,31] By the same token, when the laser is perfectly tuned with the cavity mode, where the norm of the derivative of the reflectivity presents a minimum, the detection sensitivity is exactly zero. Thus, in a standard pump-probe scheme—with similar incidence angles and identical wavelengths for the two beams—both enhancement conditions cannot be met at the same time.[31] In what follows we will introduce the experimental conditions that allow both processes to be simultaneously enhanced. These conditions are based in the double optical resonance previously used in Raman scattering.[11–14,17] The aim is to have each of the beams in the spectral position where the enhancement is maximum, that is, the pump tuned with the cavity mode dip and the probe tuned with the edge of the cavity mode. We will refer to this particular situation as double optical enhancement (DOE). For a planar semiconductor microcavity, the DOE can be accomplished by taking advantage of the continuum of in-plane optical modes. If ω_0 is the frequency of the cavity mode along the growth direction

and $k_{||}$ the photon in-plane wave vector, the mode dispersion is given by

$$\omega(k_{||}) = \sqrt{\omega_0^2 + (ck_{||}/n_{\text{eff}})^2}, \quad (1)$$

where c and n_{eff} are the speed of light and the effective index of refraction of the microcavity spacer, respectively. Thus, by increasing the angle of incidence or equivalently the $k_{||}$ the cavity mode shifts toward higher energies. Figure 2 compares the standard (a) and the DOE (b) configurations. Schematics of the experimental geometries are shown in the top panels; the simulated optical reflectivities around the microcavity mode for the pump and probe beams are plotted in the lower panels. The curves were calculated using the transfer matrix method. In both cases the pump is normal to the surface and the CM is centered at 758 nm. In case (a) the probe beam also forms a very small angle of incidence that can be approximated to zero; in case (b) the angle of incidence of the probe is larger and different from that of the pump. In the standard configuration, the reflectivity minimum for the pump (where the maximum enhancement of the coherent generation of phonons takes place) does not coincide with any of the extremes (maximum and minimum) of the derivative of the probe reflectivity. The detection becomes most efficient at these extremes. By changing the angle of incidence of the probe, it is possible to shift the maximum of the derivative to shorter wavelengths and make it coincident with the cavity mode dip of the pump reaching the DOE configuration [see Fig. 2(b)]. In this situation the generation and detection of coherent phonons are simultaneously enhanced. We performed pump-probe experiments in these two configurations.

In order to identify the relative position between laser energy and the CM in the experiment, we measured together with the coherent phonon signal the reflectivity of the laser as a function of the wavelength. In Figs. 3(a) and 3(b) we plot the optical reflectivities for the pump (orange squares) and probe (green circles) between 735 and 785 nm. The CM is located at 758 nm at normal incidence and is indicated with arrows. The continuous thick lines (green and orange) are Gaussian fits of the measurements. We also present the numerical derivative of the fit corresponding to the probe beam (thin gray line). The optical microcavity mode can be localized at ∼758 nm for the pump beam, and at ∼749 nm for the probe in the DOE configuration [Fig. 3(b)]. Observe that in the standard configuration [Fig. 3(a)] the energy of the cavity mode is identical for both beams. From Fig. 3(b) it is clear that the DOE condition is achieved [compare with the calculated reflectivity in Fig. 2(b)]. The measured FWHM of the cavity mode is ∼23 nm. This value is larger than the nominal FWHM of the mode (∼13 nm). The mode is, however, perfectly defined. At the studied wavelengths the cavity spacer is not fully transparent, and the absorption leads to a decreasing of the cavity quality factor.

In Fig. 3(c) we present the intensity of the acoustic-cavity mode as a function of the laser wavelength, when the pump is normal and the probe is almost normal to the sample surface. The weight of the signal is concentrated in the region of the optical mode and is weak outside. Two local maxima can be identified near 752 and 765 nm, which coincide with the greatest changes of the optical reflectivity as a function of wavelength; a local minimum can be identified in the cavity mode center. In addition, the signal drops to zero for wavelengths shorter than 745 nm and larger than 775 nm. When the angle of incidence of the probe beam is changed, the sensed reflectivity results modified. In Fig. 3(d) we show the intensity of the acoustic-cavity mode as a function of the laser wavelength when the probe forms an angle of incidence $\theta \sim 30^\circ$, that is, at DOE condition. In this case the CM for the probe has shifted to 750 nm. The arrow indicates the position of CM at normal incidence (pump) at 758 nm. We can identify one intense and sharp peak at 758 nm; a secondary, weaker peak at 747 nm can also be observed. The position of the main peak coincides with the CM measured with the pump, and with the maximum derivative of the reflectivity measured with the probe. This configuration corresponds to the coherent phonon generation and detection under DOE: the electric field reaches its maximal amplification in the cavity spacer enhancing the coherent phonon generation, while the probe angle senses a reflectivity that shows the maximal derivative, and thus the maximal sensitivity. The secondary peak can be related to the lower energy maximum in the detection efficiency that does not have an associated generation maximum. The signal is qualitatively different from the one in Fig. 3(c) in which both

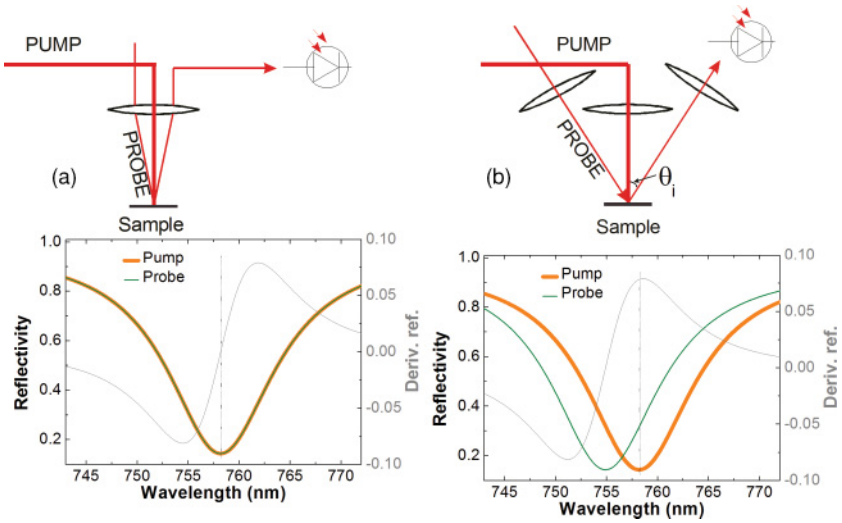

FIG. 2. (Color online) Double optical enhancement. Top panels show the experimental configuration setup. Lower panels present the reflectivity curve corresponding to the pump and probe beams (solid curves), and the derivative of the probe reflectivity (thin gray curve). (a) Standard configuration, both pump and probe have a small incidence angle. (b) Pump at normal incidence and probe with an incidence angle θ_i. The dotted vertical lines indicate the position of the optical mode in (a) and the position of the double optical enhancement in (b).

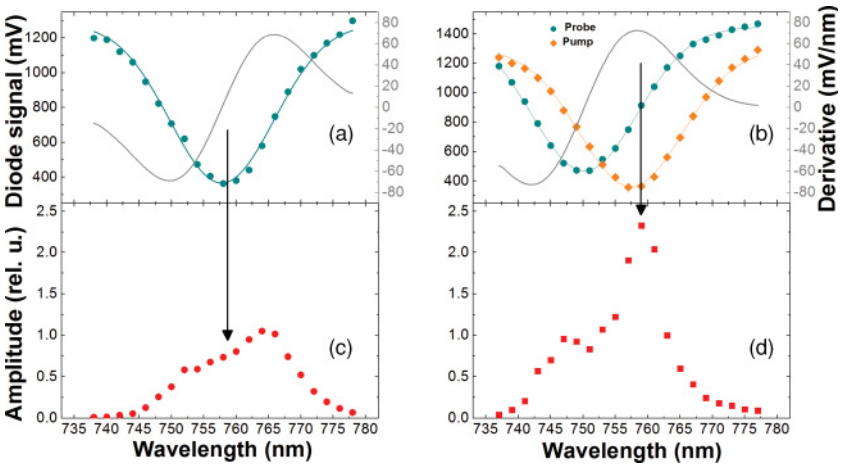

FIG. 3. (Color online) Coherent acoustic phonon generation. Top panels: optical reflectivity curves measured with the diode for both the pump (orange/thick gray) and probe (green/thin gray) beams. The thin light gray curve corresponds to the derivative of the probe reflectivity. Lower panels: acoustic cavity mode amplitude as a function of the laser wavelength. Arrows indicate the position of the microcavity mode center at normal incidence (pump beam). (a) and (c) Standard configuration, pump at normal incidence and probe with a very small angle of incidence. (b) and (d) Pump at normal incidence, and probe with an incidence angle $\theta_i \sim 30^\circ$.

peaks present a comparable intensity and there is minimum at the cavity mode dip. Additionally, the signal strongly drops for wavelengths shorter than 735 nm and larger than 770 nm; this implies that the whole weight of the signal was shifted toward shorter wavelengths, following the probe reflectivity curve. The curves in Figs. 3(c) and 3(d) were normalized to have identical values at $\lambda = 763$ nm, where the derivatives of the probe reflectivity intersect and thus an identical sensitivity is expected, while the pump efficiency remained identical in both experiments. The amplitude under DOE is a factor 2.3 larger than at $\lambda = 763$ nm. Note that this value is in good agreement with the factor 2.1 obtained from simulations. In the DOE condition the theoretical enhancement factor is 2400 with respect to a bare acoustic nanocavity sample (without optical confinement).

We introduced a DOE condition based on the usual pump-probe scheme in which a single laser (and hence wavelength) is used, varying independently pump and probe incidence angles. We presented experimental evidence on the modification of the pump-probe efficiency using the latter approach. We fixed the pump at normal incidence. We compared the wavelength dependence of the signal intensity when the angle of incidence of the probe varied from 0° to 30°, observing a clear change in the general behavior. At an angle of incidence of the probe of 30° we observed a sharp peak in the signal when the laser wavelength was tuned with the cavity mode under normal incidence. Note that in Raman scattering the optimum angle of incidence is dependent on the energy of the studied phonons; in coherent phonon generation the incidence angle only depends on the Q factor of the microcavity, that is, it is a purely optical property independent of the studied phonons. By increasing the Q factor of the cavity, the probe incidence angle needs to be reduced. The studied geometry and the achieved enhanced signals open new possibilities toward the development of novel coherent phonon sources, ultrafast optical modulation systems, and the study of structures with small photoelastic coefficients.

The authors acknowledge A. Miard for the help in growing the sample studied in this work.

*kimura@cab.cnea.gov.ar

[1] H. Yokohama, Science **256**, 66 (1992).
[2] Y. Yamamoto and R. E. Slusher, Phys. Today **46**(6), 66 (1993).
[3] M. S. Skolnick *et al.*, Semicond. Sci. Technol. **13**, 645 (1998).
[4] K. J. Vahala, Nature (London) **424**, 839 (2003).
[5] A. Fainstein and B. Jusserand, Light scattering in Solids IX: Novel Materials and Techniques **108**, 17 (2007).
[6] B. Sermage *et al.*, Phys. Rev. B **53**, 16516 (1996).
[7] D. Sanvitto *et al.*, Nat. Phys. **6**, 527 (2010).
[8] E. Wertz *et al.*, Nat. Phys. **6**, 860 (2010).
[9] G. Malpuech *et al.*, Appl. Phys. Lett. **81**, 412 (2002).
[10] G. Malpuech *et al.*, Phys. Rev. B **65**, 153310 (2002).
[11] A. Fainstein *et al.*, Phys. Rev. Lett. **75**, 3764 (1995).
[12] A. Fainstein *et al.*, Phys. Rev. B **53**, R13287 (1996).
[13] A. Fainstein and Bernard Jusserand, Phys. Rev. B **57**, 2402 (1998).
[14] M. Trigo *et al.*, Phys. Rev. Lett. **89**, 227402 (2002).
[15] N. D. Lanzillotti-Kimura *et al.*, AIP Conf. Proc. **1199**, 223 (2010).
[16] P. Lacharmoise *et al.*, Appl. Phys. Lett. **84**, 3274 (2004).
[17] N. D. Lanzillotti-Kimura *et al.*, Phys. Rev. B **79**, 035404 (2009).
[18] Ivan S. Grudinin *et al.*, Phys. Rev. Lett. **104**, 083901 (2010).
[19] R. P. Beardsley *et al.*, Phys. Rev. Lett. **104**, 085501 (2010).
[20] N. D. Lanzillotti-Kimura *et al.*, Phys. Rev. Lett. **104**, 187402 (2010).
[21] C. Thomsen *et al.*, Phys. Rev. B **34**, 4129 (1986).
[22] N. D. Lanzillotti-Kimura *et al.*, Phys. Rev. Lett. **99**, 217405 (2007).
[23] Y. Li *et al.*, J. Appl. Phys. **105**, 083516 (2009).
[24] B. Perrin *et al.*, Physica B: Condensed Matter **263-264**, 571 (1999).
[25] A. V. Scherbakov *et al.*, Phys. Rev. B **78**, 241302(R) (2008).
[26] T. Berstermann *et al.*, Phys. Rev. B **80**, 075301 (2009).
[27] T. Berstermann *et al.*, Phys. Rev. B **81**, 085316 (2010).
[28] M. M. de Lima Jr. *et al.*, Phys. Rev. Lett. **94**, 126805 (2005).
[29] M. M. de Lima Jr. *et al.*, Phys. Rev. Lett. **97**, 045501 (2006).
[30] P. D. Batista *et al.*, Appl. Phys. Lett. **92**, 133502 (2008).
[31] N. D. Lanzillotti-Kimura *et al.*, AIP Conf. Proc. **1199**, 161 (2010).
[32] Considering a purely real photoelastic constant.
[33] A. Huynh *et al.*, Phys. Rev. Lett. **97**, 115502 (2006).
[34] This thickness relation optimizes the width of the first minigap at the Brillouin zone center as shown in Ref. 35.
[35] B. Jusserand and M. Cardona, in *Light Scattering in Solids V*, edited by M. Cardona and G. Güntherodt (Springer, Heidelberg, 1989).
[36] At room temperature the optical mode is always located at higher energies than the PM and Spacer emissions.